ELECTRICAL AND PETROPHYSICAL PROPERTIES OF SILICICLASTIC RESERVOIR ROCKS FROM PORE-SCALE MODELING

Karam Ali Rezaei Gomari[1], Carl Fredrik Berg[1], Alex Mock[2], Pål-Eric Øren[2], Egil Boye Petersen Jr.[1], Alf Birger Rustad [1], Olivier Lopez[2]
[(1)]Statoil ASA and [(2)]NumericalRocks AS

This paper was prepared for presentation at the International Symposium of the Society of Core Analysts held in Austin, Texas, USA 18-21 September, 2011

ABSTRACT

In quantitative log interpretation it is common to assume that electrical conductivity is governed by Archie's law. The law is empirical and assumes a clean consolidated sand. Moreover, it also assumes that electrical conductivity is only present in the brine. Archie's law is parameterized by the cementation exponent denoted with m, and the saturation exponent denoted with n. The log interpretation requires estimation of n and m. Traditionally, petrophysical and electrical properties are obtained from laboratory experiments. In this study, we applied a direct pore-scale modeling approach to predict electrical and petrophysical properties across a wide range of rocks from the Norwegian Continental Shelf (NCS). The consistency of predicted properties was then verified against available datasets for the investigated samples.

20 siliciclastic reservoir rock samples from four different fields and four different formations of the NCS have been reconstructed using a pore scale modeling approach. For each sample, a 3D model of the rock was constructed based on thin section analysis and geological process based modeling. The reconstructed reservoir rocks have clay contents of up to 20% and well to moderately sorted grain size distributions. The permeability of the samples spans from 5mD to 2.2D and porosity from 0.14 to 0.30.

Predicted petrophysical properties include porosity, absolute permeability and formation resistivity factor (FRF). Absolute permeability was computed by solving the steady state Stoke's equation using a D3Q18 Lattice-Boltzmann algorithm. The FRF was obtained by solving the Laplace equation using a random walk algorithm. Primary drainage and water flooding resistivity index (RI) were determined from capillary dominated two-phase oil-water flow simulations on the pore network representation of the reconstructed 3D rock model. The predicted results were compared with relevant experimental data and with observed field trends.

INTRODUCTION

Saturation modeling of reservoir rocks from resistivity measurements is one of the most crucial problems in petrophysics and log analysis. The interpretations of these measurements are usually based on Archie relations. In petrophysics, Archie's law relates the *in-situ* electrical resistivity of a sedimentary rock (R_t) to its porosity (ϕ) and brine saturation (S_w):

$$R_t = \frac{a}{\phi^m}\frac{R_w}{S_w^n}$$

with a the tortuosity factor, R_w is the brine resistivity, n the saturation exponent and m the cementation exponent. Conventionally, values of both cementation and saturation exponent are most commonly assumed to be equal to 2. Significant deviations have been observed in laboratory measured data for m and n from complex lithologies. The discrepancies are mainly due to rock heterogeneity and the complicated pore structure. Pore network simulations have been recently widely used for the simulation of two-phase fluid flow in complex porous media (Caubit *et al*., 2008; Cense *et al.*, 2008; Touati *et al.*, 2009; Lopez *et al*., 2010) and can be applied to determine electrical resistivity of complex rocks such as those encountered in the petroleum industry (Blunt *et al.*, 2002, Man and Jing 2002, Bekri 2003, Knackstedt *et al.*, 2007, Tørå *et al.*, 2010).

In the present work, an integrated pore-scale modeling approach was used to reconstruct 20 siliciclastic reservoir rock samples from four different fields and four different formations from the NCS. On these 20 samples, formation resistivity factor was calculated and capillary dominated oil/water flow simulations for primary drainage have been performed and resistivity index (RI) was thus calculated. Predictions of n and m were compared with selected laboratory data and with observed field trends.

METHODOLOGY

Pore Scale Reconstruction of Reservoir Rocks

Numerical 3D sandstone reservoir rock models have been constructed based on thin section analysis and by simulating geological rock forming processes: sedimentation, compaction, and diagenesis (Øren and Bakke, 2003). Porosity of the reconstructed rocks is obtained from back scattered electron microscope (BSEM) image analysis (intergranular porosity) and a model for sub-resolution microporosity (total porosity). Absolute permeability was computed on the numerical 3D rock models using D3Q18 Lattice-Boltzmann simulations (Jin *et al.*, 2004; Øren *et al.*, 2006).

The reconstructed rock models were transformed into pore network models to retain crucial geometrical and topological properties. The data volume is hence decreased to reduce computational time. Oil/water primary drainage to irreducible water saturation S_{wi} was simulated on the extracted pore networks of each reconstructed models under fully water-wet conditions as assumed during the experiments. At the pore scale, it is assumed that the displacement processes are quasi-static and capillary dominated. This is a

reasonable assumption for low capillary number (≈10^{-6}) processes that are typical of most reservoir displacements.

Computational Method

Formation Resistivity Factor and Cementation Exponent

The calculation of the FRF is based on a solution of the Laplace equation with charge conservation (Øren and Bakke, 2002). The equations were solved using a random walk algorithm. We assign zero conductivity to the solid phase and $\sigma_w = 1$ to the brine filled pore space (i.e. resolved macroporosity). We assume that the clay associated microporosity fraction ϕ_μ remains brine saturated and assign conductivity to the microporous clay phase via Archie's law $\sigma_\mu = \sigma_w \phi_\mu^2$. We neglect surface electrical conductivity that is controlled by the cation exchange capacity of the clay minerals.

A directional formation factor is the inverse of the effective electrical conductivity. Hence, the average formation factor is calculated as the harmonic mean of the direction dependent formation factors. The cementation factor is calculated from FRF and total model porosity as

$$FRF = \phi^{-m}$$

Resistivity Index and Saturation Exponent

The resistivity index is calculated from capillary dominated two-phase flow simulations on the pore network representation of the reconstructed 3D rock model. Because Poiseuille's law is closely related to Ohm's law ($I = g_e V$), flow of electrical current is analogous to fluid flow, with pressure replaced by voltage V, fluid flow replaced by electrical current I, and hydraulic conductance replaced by electrical conductance g_e. The electrical analogy to absolute permeability is the FRF = σ_0/σ_w where σ_0 is the computed conductivity at S_w=1 and σ_w is the brine conductivity. The electrical conductance between two pore bodies is assumed to only be a function of the cross-sectional area occupied by the conducting water, $g_e = \sigma_w A_w$. Expressions for A_w for different fluid configurations, contact angles, and pore shapes are given in Øren et al., 1998. The potential field is calculated completely analogous to the pressure field (Øren et al., 1998), imposing current conservation at every pore body. The resistivity index is given by:

$$RI(S_w) = \frac{\sigma_0}{\sigma(S_w)} = S_w^{-n}$$

Experimental Data

Relevant conventional (CCA) and special core analysis (SCAL) data from the modeled fields have been used during this study. 38 core plugs from the four investigated fields have been used for this study. Conventional data, such as porosity, permeability, grain density, XRD were available and were considered to ensure the rock models represent the actual core material. The predicted properties are then directly compared to results from reconstructed samples if available otherwise from neighboring plugs. Formation factor and Pc-RI experiments were all conducted at reservoir conditions with formation fluids. All samples were cleaned before experiments and are then assumed to be fully water wet.

Primary drainage Pc-RI experiments were conducted on all samples with formation fluids. *n* was plotted as function on irreducible water saturation (S_{wi}), porosity and permeability (*k*). Clay cation exchange capacity (CEC) has been measured for samples from Field 2 with 0.017 meq.g^{-1}. For the other fields, we used a value of 0.1 meq.g^{-1} based on clay type analysis from XRD and thin section analysis. The dominant clay type for field 2 is kaolinite while for the other fields we assumed a combination of kaolinite and illite.

Variations of *m* were investigated as a function of porosity only. In addition, CCA and SCAL datasets are compared to the predicted results and trends at the field and formation level.

RESULTS AND DISCUSSION

20 siliciclastic reservoir rock samples from four different fields and four different formations of the NCS have been reconstructed using a pore scale modeling approach. Estimated porosity and permeability data were compared to conventional core analysis data from the samples used for electrical measurements. Results from the reconstructed samples are in good agreement with experimental data and with field and formation trends as shown in (Figure 1).

The samples are poorly to moderately well sorted sandstones with average grain sizes ranging from medium to very fine sand and overall sizes ranging from coarse sand to medium silt (Table 1). Diagenetic features such as quartz cementation and authigenic clay formation are important. They are modeled according to observations in BSEM images. The amount of quartz cementation is adjusted so the final intergranular porosity of the rock models agrees with the observations in the BSE image (see Table 2). Fractions of clay minerals in the rock models are listed in Table 2. The distribution of clay minerals (pore filling vs. matrix associated) and the porosity distribution (inter- vs. intra-granular) are also modeled according to BSEM image observations.

The m-exponent for each field was calculated using a least square regression for ln(FRF) = -m ln(ϕ). Similarly, the n-exponent for each sample was calculated using a least square regression for ln(RI) = -n ln(Sw), while the field value is the mean of the individual samples.

Field 1

Five samples from one formation were selected from field 1. The total porosity range is from 0.149 to 0.163 and the permeability range is from 57mD to 162mD. These samples have relatively low clay content, ranging from 2 to 6%.

The average value for the cementation exponent *m* of the 5 reconstructed samples from Field 1 is 2.03. This result is in good agreement with the available experimental data *m*=1.96 for this field. Simulated *m* span from 1.85 to 2.14 and tends to decrease with

increasing porosity, while experimental data span from 1.85 to 2.02 for the same range of porosity.

Comparison of *RI* simulated for sample 1B and experimental data of Field 1 are summarized in Figure 2. The average value for the simulated saturation exponent *n* is 2.09 for the 5 reconstructed samples and matches very well the experimental value of 2.04.

Simulated cementation exponents tend to be slightly higher than experimental data while saturation exponent are well in line with experiments as shown in Figure 3.

Field 2

Five samples from one formation were selected from field 2. Porosity and permeability ranges are from 0.144 to 0.285 and from 57mD to 1.1D respectively. The clay content for these samples is from 5 to 10%.

The average *m* of the 5 reconstructed samples from Field 2 is 1.95, which is in excellent agreement with the available experimental data *m*=1.95 for this field. Simulated *m* vary from 1.85 to 2.05 while experimental data vary from 1.83 to 2.09 as shown in Figure 4.

The average value for calculated *n* is 2.94. There is a large variation in the experimental data for saturation exponent, from 1.93 to 3.39, with an average value of 2.80. Simulated saturation exponents are well in line with experimental data trends (Figure 4). The dominant clay type for field 2 is kaolinite and available CEC measurements show an average value of 0.017 $meq.g^{-1}$. This value is low compared to the assumed value for the other fields (0.1 $meq.g^{-1}$) and leads to higher overall resistivity.

Field 3

Five samples from one formation were selected from field 3. They are the most porous samples of the study with a total porosity ranging from 0.255 to 0.301. The permeability range is from 82mD to 2.2D. The clay content is from 5 to 11%.

Results are summarized in Figure 5 for Field 3. The average *m* of the 5 reconstructed samples is 1.89. This is in good agreement with the experimental cementation exponent *m*=1.82 for the field. Simulated *m* is from 1.81 to 1.99 while experimental data is from 1.77 to 1.84. At low porosity, the simulated *m* tends to be higher than experimental ones. The average value for the simulated saturation exponent *n* is 2.22 while experimental *n* is 2.05. Average simulated saturation exponent are slightly higher than experimental data at low porosity. Experimental *n* and *m* data show no particular trend with respect to the investigated parameters.

Field 4
Five samples from one formation were selected from field 4. The total porosity range is from 0.160 to 0.183 and the permeability range is from 5mD to 669mD. These samples have clay content from 2 to 8%.

The average *m* of the 5 reconstructed samples from Field 4 is 1.92, while experimental cementation exponent is *m*=1.86. Simulated *m* vary from 1.83 to 2.01 while experimental data is from 1.81 to 1.89. Results are summarized in Figure 6.

The average value for the simulated saturation exponent *n* is 2.12, lower than the experimental value of 2.41. Both experimental and simulated *n* are following the same trends.

Comparison of all simulated and experimental data is summarized in Figure 7. Trends defined by experiments are well reproduced by simulated results. No offset from simulations is observed.

CONCLUSION
A pore scale modeling approach has been applied on 20 siliciclastic reservoir rock samples to estimate their electrical properties. Estimated Archie's cementation exponent *m* from grid model are in good agreement with experimental data and trends.

Saturation exponents estimated from primary drainage capillary dominated water/oil flow simulations are also in good agreement with experimental data and trends.

The presented applied pore-scale modeling approach offers a reliable technique to estimate electrical property data for siliciclastic rocks over the investigated range of porosity (0.14 to 0. 30) and permeability (5mD to 2.2D).

ACKNOWLEDGEMENTS
This study was part of a Statoil internal project and the authors would like to thank Statoil for permission to publish this work.

REFERENCES
1. Bekri, S., Howard, J., Muller, J. and Adler, P.M. “Electrical Resistivity Index in Multiphase Flow through Porous Media”, *Transport in Porous Media* (2003) **51**, 41-65.
2. Blunt, M., Jackson, M.D., Piri M., Valvatne, Per.H. “Detailed physics, predictive capabilities and macroscopic consequences for pore network models of multiphase flow”, *Advances in Water Resources* (2002) **25**, 1069-1089.

3. Caubit, C., Hamon, G., Sheppard, A.P. and Øren, P.E. "Evaluation of the reliability of prediction of petrophysical data trough imagery and pore network modelling", paper SCA2008-33 presented at the 2008 SCA International Symposium, Abu Dhabi, 29 Oct.-2 Nov.
4. Cense, A. and Marcelis, F. "A comparative study of three pore-scale reconstruction and pore-network extraction technique", paper SCA2008-36 presented at the 2008 SCA International Symposium, Abu Dhabi, 29 Oct.-2 Nov.
5. Jin, G., Patzek, T.W. and Silin, D.B. "Direct Prediction of Absolute Permeability of Unconsolidated and Consolidated Reservoir Rock", paper SPE 90084 presented at the SPE ATCE, Houston, TX, September 2004.
6. Knackstedt, M.A., Arns, C.H., Sheppard, A. P., Senden, T.J., Sok, R.M., Cinar, Y., Olafuyi, A.O., Pinczewski , W.V., Padhy, G. and Ioannidis, D. "Pore scale analysis of electrical resistivity in complex core material ", paper SCA2007-33 presented at the 2007 SCA International Symposium, Calgary, 10-12 September..
7. Lopez, O., Mock, A., Skretting, J., Petersen, E.B.Jr, Øren, P.E. and Rustad, A.B. "Investigation into the reliability of predictive pore-scale modeling for siliciclastic reservoir rocks", paper SCA2010-41 presented at the 2010 SCA International Symposium, Halifax, 4-7 October.
8. Man, H.N. and Jing, X.D. "Network modelling of mixed wettability on electrical resistivity, capillary pressure and wettability indices", *Journal of Petroleum Science and Engineering* (2002) **33**, 101-122.
9. Touati, M., Suicmez, S., Funk, J., Cinar, Y. and Knackstedt, M. "Pore Network Modeling of Saudi Aramco Rocks: A Comparative Study", paper SPE 126043 presented at the 2009 SPE Saudi Arabia Section Technical Symposium and Exhibition, Al Khobar, May 2009.
10. Tørå, G., Hansen, A. and Øren, P.E. "Dynamic network modeling of resistivity index in a steady-state procedure", paper SPE 135367 presented at the 2010 SPE Annual Technical Conference and Exhibition, Florence, Italy, September 2010.
11. Øren, P.E. and Bakke, S. "Reconstruction of Berea Sandstones and Pore-Scale Modeling of Wettability Effects", *J. Petroleum Science & Engineering* (2003) **39**, 177-199.
12. Øren, P.E., Bakke, S. and Arntzen, O.J. "Extending Predictive Capabilities to Network Models", *SPEJ* (1998), 324-336.
13. Øren, P.E. and Bakke, S. "Process Based Reconstruction of Sandstones and Prediction of Transport Properties", *Transport in Porous Media* (2002) **46**, 311-343.
14. Øren, P.E., Bakke, S. and Rueslåtten, H.G. "Digital core laboratory: Rock and flow properties derived from computer generated rocks", paper SCA2006-21 presented at the 2006 SCA International Symposium, Trondheim, 12-16 September.

Table 1. Characteristics of 3D grain size distributions extracted from BSEM thin section images.

Field	Sample	Mode [µm]	Mean [µm]	St. Dev. [µm]	Max. size [µm]	Min. size [µm]
1	1A	177	134	86	559	54
1	1B	157	162	106	300	45
1	1C	121	126	83	350	44
1	1D	125	103	65	500	60
1	1E	69	80	63	300	40
2	2A	129	127	84	204	37
2	2B	281	310	206	569	56
2	2C	282	289	189	508	102
2	2D	250	219	95	890	40
2	2E	177	196	128	713	40
3	3A	65	65	43	99	41
3	3B	102	103	67	144	77
3	3C	113	115	75	170	47
3	3D	81	83	54	135	46
3	3E	281	278	183	490	107
4	4A	113	131	89	456	39
4	4B	103	105	69	194	38
4	4C	107	111	73	194	38
4	4D	183	202	134	441	39
4	4E	182	260	172	471	36

Table 2. Predicted results from simulations for the 20 samples (3 realizations per sample); IG = intergranular.

Field	Sample	ϕ IG	ϕ total	k in [mD]	n	FRF	m	Clay frac.
1	1A	0.144	0.154	162	1.83	46.5	2.05	0.02
1	1B	0.140	0.155	81	2	39.3	1.97	0.03
1	1C	0.119	0.149	72	2.41	54.3	2.06	0.06
1	1D	0.144	0.154	57	2.08	54.5	2.14	0.02
1	1E	0.138	0.163	148	2.11	30.8	1.85	0.05
2	2A	0.129	0.174	57	3.6	33.6	2.05	0.09
2	2B	0.189	0.239	415	2.88	14.1	1.85	0.10
2	2C	0.119	0.144	87	2.8	49.3	2.01	0.05
2	2D	0.192	0.237	513	2.81	14.7	1.87	0.09
2	2E	0.245	0.285	1101	2.6	10.9	1.86	0.08
3	3A	0.230	0.255	156	2.17	13.9	1.93	0.05
3	3B	0.235	0.261	417	2.05	12.5	1.88	0.05
3	3C	0.261	0.301	1119	2.05	9.2	1.84	0.08
3	3D	0.189	0.244	82	2.59	16.3	1.99	0.11
3	3E	0.236	0.291	2238	2.22	9.3	1.81	0.11
4	4A	0.157	0.183	94	2.1	26.6	1.93	0.05
4	4B	0.120	0.16	8	2.71	39.5	2.01	0.08
4	4C	0.102	0.142	5	2.5	40.7	1.9	0.08
4	4D	0.156	0.176	352	1.7	24.1	1.83	0.04
4	4E	0.167	0.177	669	1.57	28	1.93	0.02

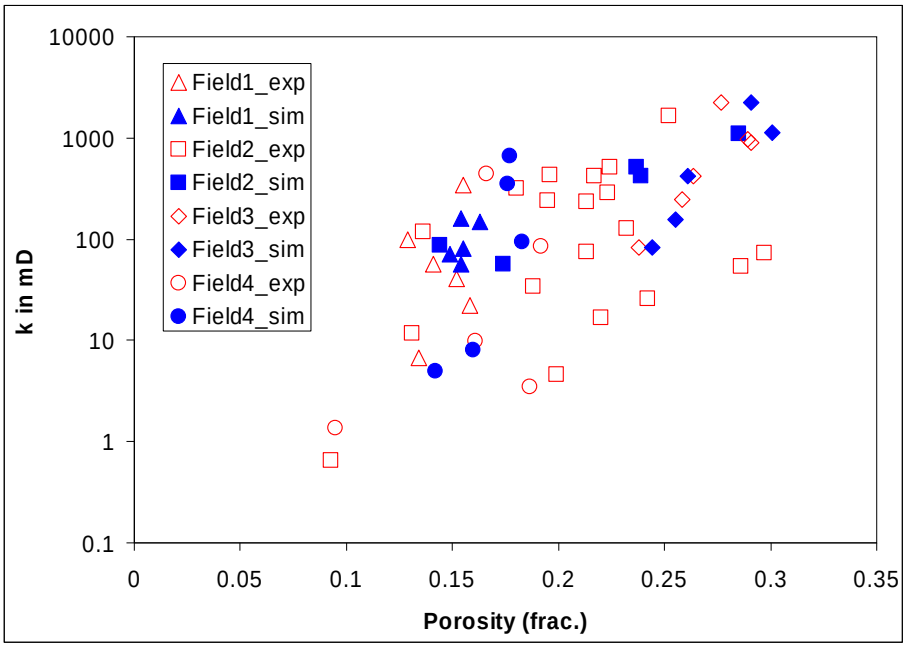

Figure 1. Cross plot of porosity (fraction) as a function of permeability (in mD) for simulated (filled symbols) and laboratory (open symbols) experiments.

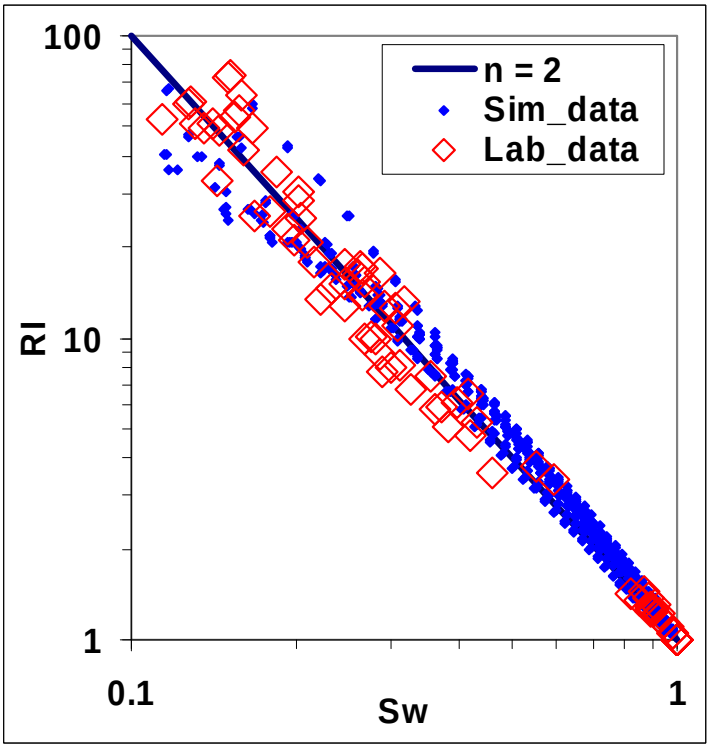

Figure 2. Resistivity index of sample 1B during primary drainage. Simulated results are filled symbols and laboratory measurements open symbols.

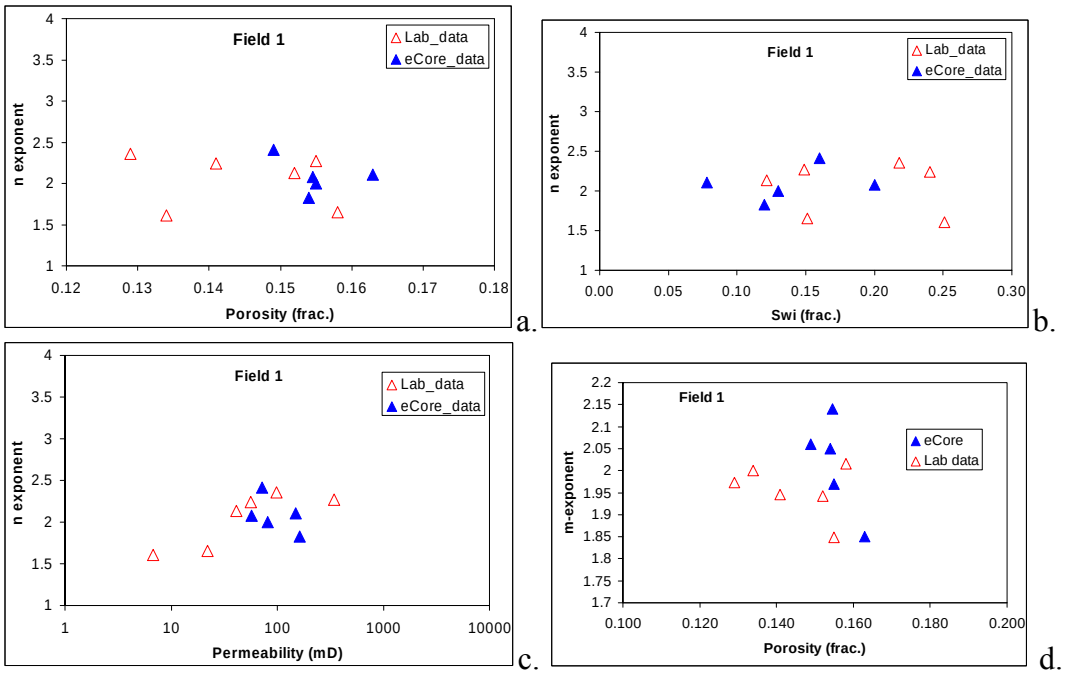

Figure 3. Cross plots of *n* and *m* for Field 1 with open symbols for laboratory measurements and filled symbols for simulated data. a. *n* vs. porosity (fraction), b. *n* vs. S_{wi}, c. *n* vs permeability in mD and d. *m* vs. porosity (fraction).

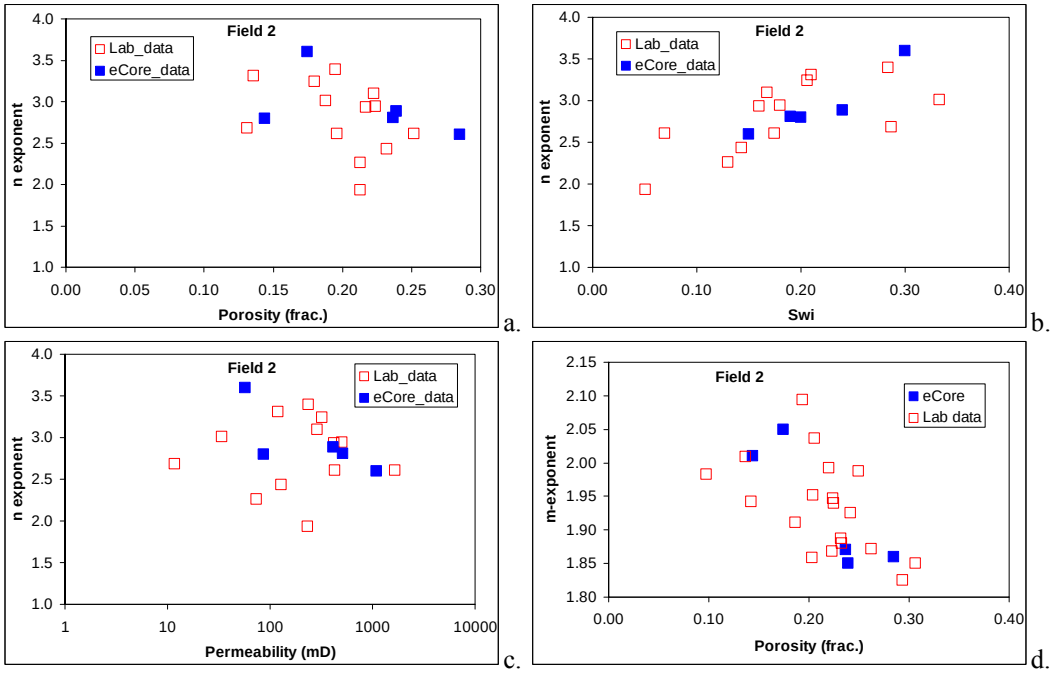

Figure 4. Cross plots of *n* and *m* for Field 2 with open symbols for laboratory measurements and filled symbols for simulated data. a. *n* vs. porosity (fraction), b. *n* vs. S_{wi}, c. *n* vs permeability in mD and d. *m* vs. porosity (fraction).

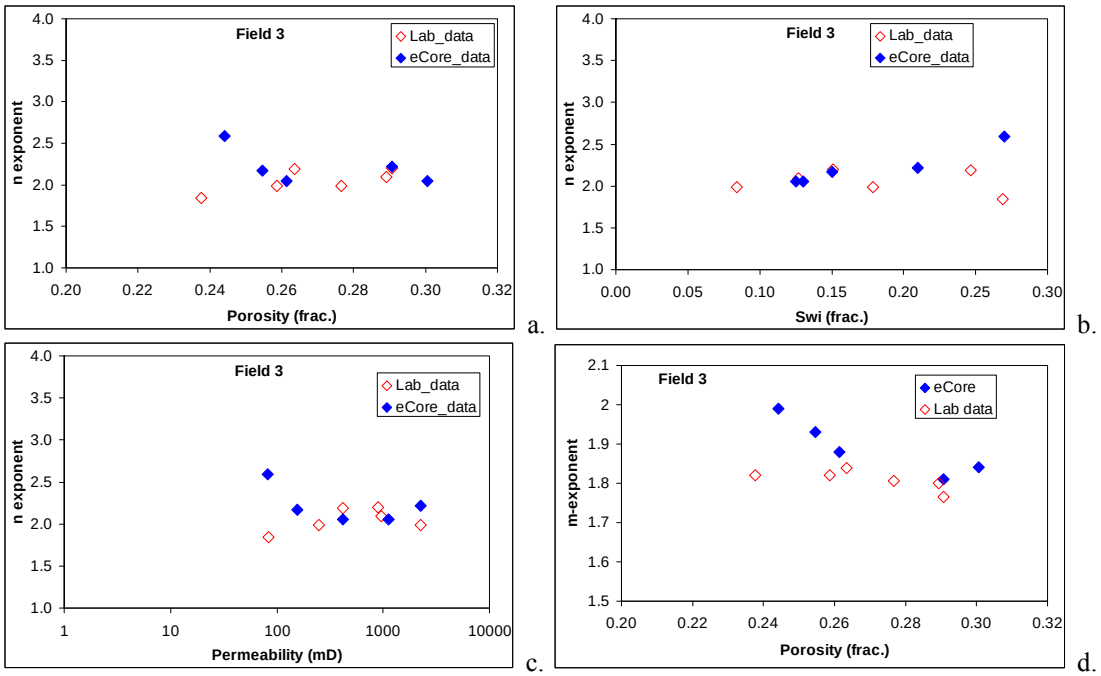

Figure 5. Cross plots of *n* and *m* for Field 3 with open symbols for laboratory measurements and filled symbols for simulated data. a. *n* vs. porosity (fraction), b. *n* vs. S_{wi}, c. *n* vs permeability in mD and d. *m* vs. porosity (fraction).

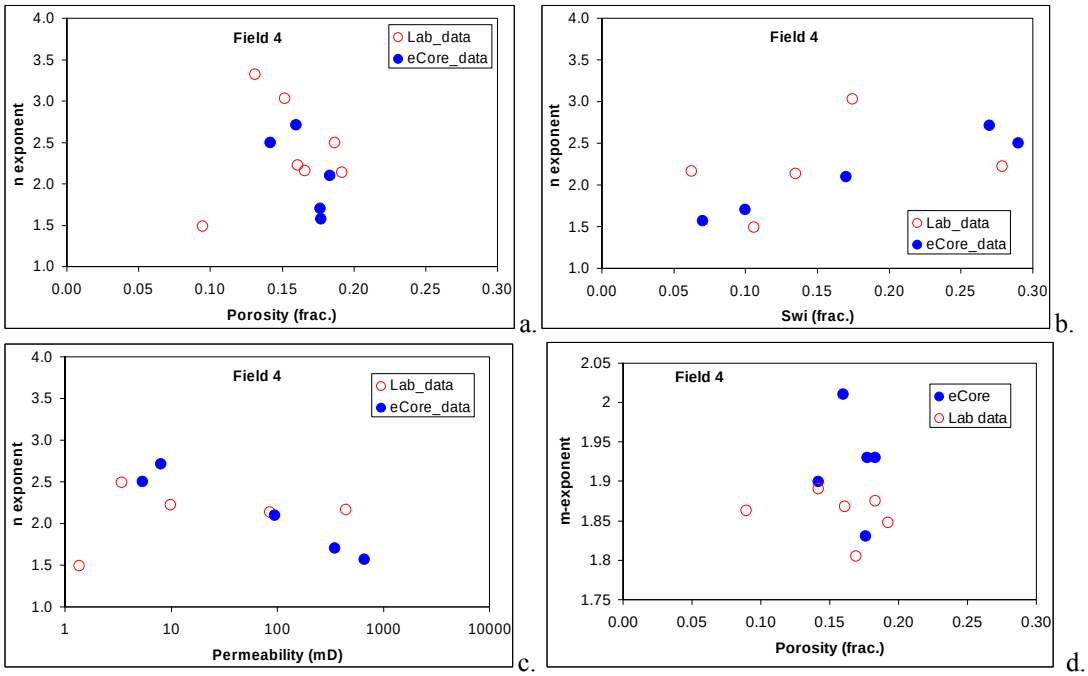

Figure 6. Cross plots of *n* and *m* for Field 4 with open symbols for laboratory measurements and filled symbols for simulated data. a. *n* vs. porosity (fraction), b. *n* vs. S_{wi}, c. *n* vs permeability in mD and d. *m* vs. porosity (fraction).

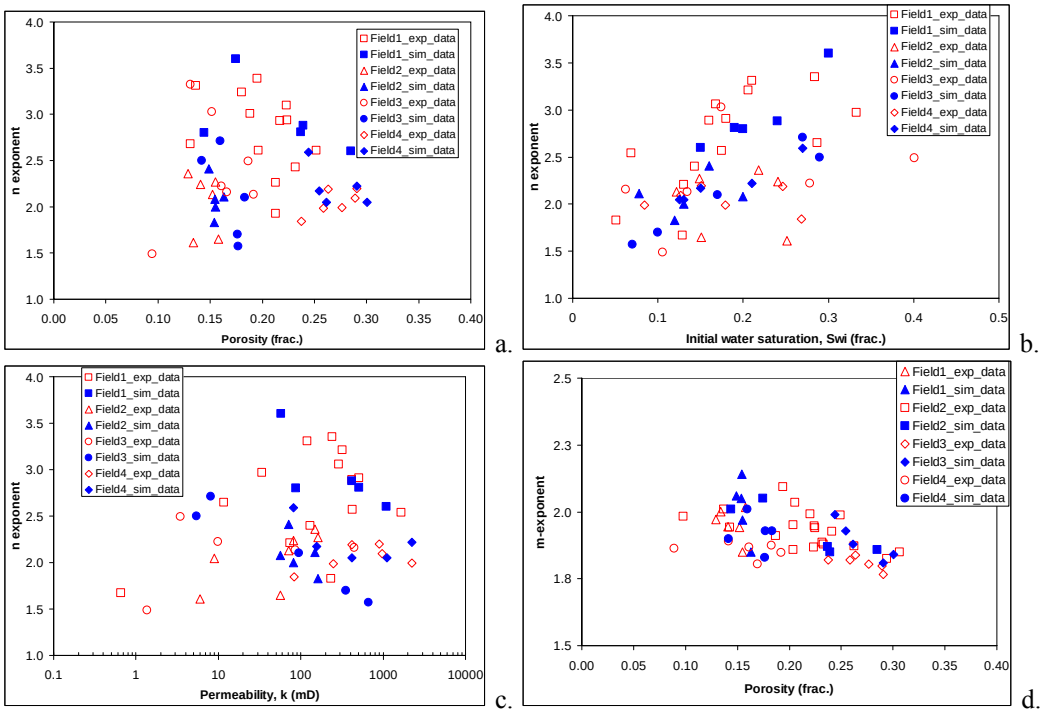

Figure 7. Cross plots of *n* and *m* for all investigated fields with open symbols for laboratory measurements and plain symbols for simulated data. a. *n* vs. porosity (fraction), b. *n* vs. S_{wi}, c. *n* vs permeability in mD and d. *m* vs. porosity (fraction).